

Integrated Sensing and Communications towards Proactive Beamforming in mmWave V2I via Multi-Modal Feature Fusion (MMFF)

Haotian Zhang, *Graduate Student Member, IEEE*, Shijian Gao, *Member, IEEE*,
Xiang Cheng, *Fellow, IEEE*, Liuqing Yang, *Fellow, IEEE*,

Abstract

The future of vehicular communication networks relies on mmWave massive multi-input-multi-output antenna arrays for intensive data transfer and massive vehicle access. However, reliable vehicle-to-infrastructure links require narrow beam alignment, which traditionally involves excessive signaling overhead. To address this issue, we propose a novel proactive beamforming scheme that integrates multi-modal sensing and communications via Multi-Modal Feature Fusion Network (MMFF-Net), which is composed of multiple neural network components with distinct functions. Unlike existing methods that rely solely on communication processing, our approach obtains comprehensive environmental features to improve beam alignment accuracy. We verify our scheme on the ViWi dataset, which we enriched with realistic vehicle drifting behavior. Our proposed MMFF-Net achieves more accurate and stable angle prediction, which in turn increases the achievable rates and reduces the communication system outage probability. Even in complex dynamic scenarios, robust prediction results can be guaranteed, demonstrating the feasibility and practicality of the proposed proactive beamforming approach.

This work was supported in part by the National Natural Science Foundation of China (Grants No. 62125101 and 62341101). Haotian Zhang and Xiang Cheng are with the State Key Laboratory of Advanced Optical Communication Systems and Networks, School of Electronics, Peking University, Beijing 100871, China (e-mail: haotianzhang@stu.pku.edu.cn; xiangcheng@pku.edu.cn).

Shijian Gao is with the Samsung Semiconductor, Samsung SoC Research and Development Lab, San Diego, CA 92121 USA (e-mail: gao00379@umn.edu).

Liuqing Yang is with the Internet of Things Thrust and Intelligent Transportation Thrust, The Hong Kong University of Science and Technology (Guangzhou), Guangzhou 510000, China, and also with the Department of Electronic and Computer Engineering and the Department of Civil and Environmental Engineering, The Hong Kong University of Science and Technology, Hong Kong, SAR, China (e-mail: lqyang@ust.hk).

Index Terms

Vehicular communication networks, multi-modal sensing-communication integration, mmWave, proactive beamforming, deep learning, vehicle-to-infrastructure.

I. INTRODUCTION

The vehicular communication network (VCN) is playing an increasingly important role in intelligent transportation systems [1]–[3]. To meet the ultra-reliable and low latency communication requirements of VCN applications [4], [5], millimeter-wave (mmWave) communications have been recognized as one of the key enablers for 5G and beyond wireless systems [6]–[8]. To compensate for the high path loss in the mmWave band and reduce interference to non-target users [9]–[11], the transmitter typically deploys a massive multi-input-multi-output (mMIMO) antenna array and formulates “pencil-like” beams to focus energy on the directions of users. Due to the narrow beamwidth, it is crucial to align the transmit and receive beams between the road side unit (RSU) and vehicles to establish a reliable vehicle-to-infrastructure (V2I) communication.

Conventional beam alignment methods generally design the precoding matrix based on dedicated beam training [12]–[16]. The typical solution involves the search for the beam pair with the strongest signal-to-noise ratio (SNR) by exhaustively sweeping all beams in the codebook [12], [13]. However, the subsequent high overhead makes it impractical for VCN, where the beamforming angle and the precoding matrix need to be predicted and updated frequently due to potentially frequent channel variations [17]. To overcome this deficiency, *beam tracking* [14] has been proposed to reduce the search space of the optimal beam pairs by utilizing temporal correlation. Despite this improvement, periodic signaling interaction still brings huge latency and overhead. To further reduce the pilots, *proactive beamforming* has recently been proposed to avoid frequent training from the scratch. Existing proactive beamforming schemes generally adopt simple kinematic models and take up additional spectrum resources to conduct motion detection or state feedback [18]–[23]. The existing works on proactive beamforming mainly rely on state evolution models, such as the Kalman filter or its extended version [18], [19], to track the vehicle’s motion parameters. However, these methods are subject to approximations due to the high nonlinearity of the state evolution model, which limits the prediction accuracy.

To address this limitation, researchers have started exploring alternative methods that rely on deep learning (DL) techniques. Specifically, [22], [23] has been utilized to vehicle’s motion

prediction and beamforming matrix prediction with receive signals and historical estimated channels serving as input. To make the application scenarios more generic, Liu *et al.* [24] proposed a maximum likelihood estimator-based scheme using the vehicle’s historical trajectory data rather than a state evolution model. Though the above schemes partially address the problem of predicting the vehicle’s angular parameter, they primarily utilize the electromagnetic propagation environment information to learn the vehicle’s motion parameter evolution characteristic. This limitation restricts the application of such schemes in complex and dynamic environments.

Fortunately, with the increasing prevalence of advanced sensors in intelligent transportation infrastructure, various studies have explored the integration of multi-modal sensing into communication system design [25]–[33]. For instance, Alrabeiah *et al.* [25] proposed to utilize RGB images to aid mmWave beam and blockage prediction tasks in VCN. Demirhan *et al.* [26] developed beam prediction schemes based on radar raw data, range-angle maps, and range-velocity maps. In [27] and [28], the LiDAR point cloud was leveraged for beam selection and link blockage prediction tasks. Xu *et al.* [29] designed a vision-aided channel covariance matrix estimation method that used onboard camera images to improve the estimation accuracy. Charan *et al.* [30] combined image frames and mmWave beams to proactively predict blockages. Moreover, Fan *et al.* [32] has extended the application of sensing-aided beamforming to a multi-hop vehicle-to-vehicle network.

The works discussed in [25]–[33] utilize uni-modal sensory data, which falls short in offering comprehensive environmental features and yields limited gains in communication functionalities. Furthermore, the non-RF sensors are sensitive to harsh weather and lighting conditions, causing the uni-modal sensor-based schemes to fail in certain cases. Recently, [3] raises that multi-modal sensing can potentially reflect the channel propagation characteristics and help with multi-layer and multi-objective communication functionalities. Furthermore, inspired by human synesthesia, [3] proposes that the multi-modal sensors can be referred to as “machine senses” and the multi-modal sensing-communication integration implies synesthesia of “machine senses” in various RF and non-RF formats. However, merely combining multi-modal data is far from sufficient in real use, thus advanced data processing and feature analysis require an in-depth investigation. Firstly, efficient data pre-processing methods for multi-modal data with different semantic information and data structures must be developed to extract relevant features and eliminate redundant information. Secondly, dedicated DL models capable of extracting multi-modal features and fusing them need to be explored. To this end, we propose a Multi-Modal Feature Fusion Network

(MMFF-Net) which includes three judiciously designed feature extraction modules, a multi-modal feature fusion mechanism, and two distinct regression models for predicting the angle of vehicles. Our main contributions are summarized as follows:

- The proposed scheme integrates multi-modal sensing with communications through a **dedicated neural network (NN) construction** for proactive beamforming. This approach utilizes multi-modal feature extraction and fusion modules to obtain motion characteristics of a vehicle, allowing for a synesthetic framework of “machine senses.” The MMFF-Net accurately predicts a vehicle’s future position, and includes two regression models to accommodate the high-dimensional input and the vehicle’s random drifting behavior. The proposed scheme is suitable for scenarios where the vehicle drifts randomly while driving.
- The dataset is enriched with dynamic scenarios to expand the applicability of proactive beamforming. It is constructed based on the ViWi data-generation framework [34] and further enhanced by considering the vehicle’s **random drifting behavior**. Each trajectory point in the dataset is accompanied by synchronized RGB images, depth maps¹, and CSI. The proposed scheme has been proven to efficiently support more complicated and realistic scenarios.
- The proposed scheme outperforms up to **nine** benchmark schemes in terms of the prediction accuracy and adaptability to the vehicle’s behavior. MMFF reduces the angle prediction error by more than 35 percent in comparison with the benchmark schemes when the vehicle approaches RSU and relative angle varies fast. This in turn leads to an **achievable rate gain of 5.8 percent** when a large antenna array is adopted. Additionally, the proposed scheme minimizes the outage probability of the communication system when adopted. The proposed algorithm will be made open source, providing a reference point for future research.

The remainder of this paper is organized as follows. Section II introduces the scenario considered and the proactive beamforming problem to be solved in this paper. Section III presents the operation process of the multi-modal feature extraction modules. Section IV details the multi-modal feature fusion, temporal feature extraction, and recurrent prediction. Section V provides the description of the experimental setup to verify the proposed scheme. Section VI presents extensive simulation results and analyses. The conclusion is drawn in Section VII.

¹Note that depth maps added with Gaussian noise are used for mimicking frequent radar sensing results throughout this paper.

Notations: Throughout this paper, we use a capital boldface letter \mathbf{A} , a lowercase boldface letter \mathbf{a} , and a lowercase letter a to represent a matrix, a vector, and a scalar, respectively. $\mathbb{C}^{M \times N}$ represents a complex space of dimension $M \times N$ and $\mathbb{R}^{M \times N \times K}$ represents a real space of dimension $M \times N \times K$. \mathbf{A}^{-1} , \mathbf{A}^T , and \mathbf{A}^H represent the inverse, transpose, and the Hermitian transpose of \mathbf{A} , respectively. $|\cdot|$ represents the modulus of a complex number. The notations \otimes and \oplus represent the matrix element-wise product and the concatenation operation, respectively. Given vectors $\mathbf{a} \in \mathbb{C}^{1 \times M}$ and $\mathbf{b} \in \mathbb{C}^{1 \times N}$, $\mathbf{a} \oplus \mathbf{b} = [\mathbf{a}, \mathbf{b}] \in \mathbb{C}^{1 \times (M+N)}$.

II. SCENARIO AND PROBLEM DESCRIPTION

In this section, we provide a high-level overview of the VCN scenario studied in this paper. Subsequently, we describe the proactive beamforming problem that we aim to address.

A. Scenario

In this paper, we consider a VCN scenario where an RSU is serving a passing vehicle. We assume that the C/U-plane decoupled network architecture is adopted, which integrates sub-6 GHz bands and broadband mmWave bands to expand the system bandwidth. The control channel is assumed to operate at sub-6 GHz bands and transmit control information between the vehicle and RSU. The data channel is assumed to operate at mmWave bands and transmit user data. As depicted in Fig. 1, the RSU is equipped with a MIMO uniform linear array (ULA) which operates at both mmWave band and sub-6 GHz band with N_t^{HF} transmit antennas at mmWave band, and N_t^{LF} transmit antennas at sub-6 GHz band. The vehicle is assumed to be equipped with a MIMO ULA which also operates at both the mmWave band and sub-6 GHz band with M_r^{HF} receive antennas at mmWave band and single antenna at sub-6 GHz band. The communication system is assumed to adopt the orthogonal frequency division multiplexing (OFDM) technique with K_{HF} subcarriers at the mmWave band and K_{LF} subcarriers at the sub-6 GHz band. In order to collect real-time multi-modal sensory data, the RSU is also equipped with an RGB-D camera. The depth data (the distances from the object to the depth camera) added with Gaussian noise is used to mimic frequent radar sensing.

B. Problem Description

In order to achieve ultra-reliable communications in latency-critical VCNs, it is crucial for RSUs to acquire accurate relative angles of passing vehicles in real time, and formulate a narrow

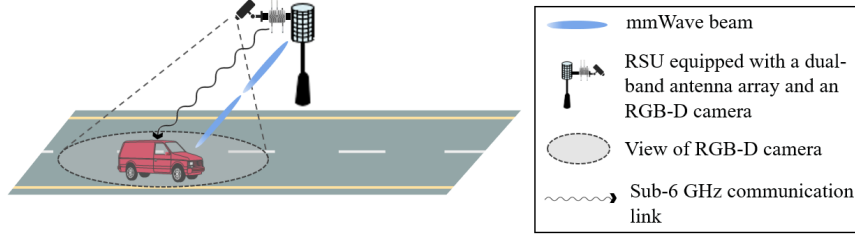


Fig. 1. The communication scenario involves an RSU serving a passing vehicle: RSU is equipped with dual-band sub-6 GHz and mmWave transceivers, as well as an RGB-D camera; the passing vehicle is also equipped with dual-band sub-6 GHz and mmWave transceivers.

transmit beam that accurately points to the vehicle. However, conventional beam training and tracking methods can cause high signaling overhead and latency. To overcome this, RSUs can predict the beamforming angle in the next time slot, without requiring extra signaling interaction or exhaustive search.

To further optimize this process, we propose utilizing multi-modal sensory data and wireless channel data to assist the RSU in achieving the above goal. Specifically, RSU senses the traffic environment at a fixed frequency and communicates with the passing vehicle constantly. At the n -th time slot, RSU predicted the relative angle $\hat{\theta}_{n+1}$ at the passing vehicle using the RGB images, depth maps, and CSI of sub-6 GHz channel. To achieve this, dedicated pre-processing methods for multi-modal data and feature fusion methods based on DL model need to be developed. Note that the vehicle also needs to formulate the narrow beam that points to RSU based on the angle prediction result when it adopts a MIMO ULA. We assume that RSU with more computing power conducts the angle prediction and sends the result to the vehicle by the current communication link. With the angle prediction result $\hat{\theta}_{n+1}$, both the RSU and vehicle accordingly formulate the narrow beams using the transmit beamforming matrix $\mathbf{f}_n = \mathbf{a}(\hat{\theta}_{n+1})$ and receive beamforming matrix $\mathbf{w}_n = \mathbf{b}(\hat{\theta}_{n+1})$, respectively. $\mathbf{a}(\theta)$ and $\mathbf{b}(\theta)$ are the transmit steering vector of the RSU's antenna array and receive steering vector of the vehicle's antenna array, respectively. The goal of a desirable proactive beamforming scheme is to predict the future relative angle as accurately as possible and maintain stable results when facing realistic random behavior, thus maximizing the achievable rate and reducing the outage probability of the communication system.

III. MULTI-MODAL FEATURE EXTRACTION

While serving the passing vehicle, RSU continuously senses the traffic environment. At each slot, it proactively predicts the future position of the vehicle and optimizes beamforming using multi-modal sensory data and wireless channel data. However, multi-modal data has distinct semantic information and data formats, which calls for dedicated data pre-processing and feature extraction that relate to vehicle motion parameters. To address this, we design a novel MMFF-Net consisting of three distinct feature extraction modules, each utilizing different data pre-processing methods and containing NNs with distinct architectures and functions. For simplicity, in the following content, all subscripts n refer to certain data at the n -th time instance and will not be reiterated.

A. Angular Feature Extraction Module

CSI can be regarded as the compressed electromagnetic environment characterization, which is roughly characterized by the relative angle at the passing vehicle. Therefore, we define the angular feature related to the LoS channel's azimuth. Benefiting from the angular feature, the NN can learn the vehicle's motion state evolution characteristics more efficiently and predict the future position more accurately.

However, obtaining the angular feature faces challenges. First, the MIMO and OFDM techniques jointly lead to a large CSI matrix which causes the high processing load of NN and long training time. Second, the acquisition of CSI in mmWave bands requires excessive signaling overhead and time to transmit sufficient training symbols due to the limited RF chains in the commonly adopted hybrid structure. Third, raw CSI does not explicitly reflect the angular information of the signal transmission paths though it is a joint result of them. In response to these challenges, we design an angular feature extraction (AFE) module to pre-process the raw CSI into a low-dimensional one and extract the implied angular feature. To avoid the excessive signaling overhead and latency, we assume that RSU obtains the CSI through necessary control signaling (such as synchronous signal) transmitted at sub-6 GHz bands. Though the MIMO beamforming is conducted at mmWave bands, CSI of sub-6 GHz bands can still reflect the similar signal propagation process with that of mmWave bands, especially the LoS component [35]. Therefore, it can provide rough angular information of vehicle in the electromagnetic domain. In what follows, we will introduce the pre-processing methods of raw CSI and the extraction of the angular feature.

1) *Pre-Processing of Raw CSI*: The AFE module is dedicated to transforming the primitive CSI matrix into a representation with explicit angular features, achieved through *energy calculation* and *dimensionality reduction* in the angle domain. First, a pre-defined angular dictionary matrix $\mathbf{D} = \{\mathbf{d}_1, \mathbf{d}_2, \dots, \mathbf{d}_B\}$ is used to calculate the total energy of all subcarriers at each beam angle, where $\mathbf{d}_b \in \mathbb{C}^{N_t^{LF} \times 1}$ and B denote the b -th beamforming vector and angle resolution, respectively. Let $\mathbf{H}_n \in \mathbb{C}^{N_t^{LF} \times K_{LF}}$ be the CSI matrix at sub-6 GHz band, $\mathbf{H}_n[k] \in \mathbb{C}^{N_t^{LF} \times 1}$ be the sub-6 GHz channel of the k -th subcarrier, and $\mathbf{h}_n^P \in \mathbb{R}^{B \times 1}$ be the processed CSI matrix after *dimensionality reduction* and *energy calculation* in angle domain. Then, $\mathbf{h}_n^P[i]$ is the i -th element of \mathbf{h}_n^P which represents the achievable rate averaged across all subcarriers at the i -th beam and can be calculated as

$$\mathbf{h}_n^P[i] = \frac{1}{K_{LF}} \sum_{k=1}^{K_{LF}} \log_2 (1 + \rho |\mathbf{d}_i^T \mathbf{H}_n[k]|^2) \quad (1)$$

where ρ denotes the SNR. By (1), the data rates achieved by different steering vectors in the dictionary matrix between the passing vehicle and the RSU are obtained. As the steering vector angle gets closer to the relative angle between the RSU and the passing vehicle, the achievable rate increases. Therefore, the significant differences among the values in \mathbf{h}_n^P effectively reflect the relative angular feature between the passing vehicle and the RSU. Table I gives an example of the average achievable rates using different steering vectors in the dictionary matrix based on (1) in our simulation.

TABLE I

THE ACHIEVABLE RATE AVERAGED ACROSS ALL SUBCARRIERS AT DIFFERENT BEAM ANGLES IN THE DICTIONARY MATRIX.

Beam index	1	2	...	16	17	18	19	20	21	22	23	24	...	64
Average achievable rates	0.02	0.03	...	0.79	0.78	0.66	1.69	2.42	3.27	5.26	1.69	0.81	...	0.02

To highlight the angular feature and boost the NN's learning capability, only the top-8 largest elements in \mathbf{h}_n^P are retained, and the other elements are set to 0. We refer to this operation as *zero-forcing of low-energy beams*. The rationality of retaining the top-8 largest elements to enhance the angular feature will be demonstrated in the next subsection. Let δ be the eighth-largest element in \mathbf{h}_n^P , the ultimate pre-processed CSI matrix $\mathbf{h}_n^{P'} \in \mathbb{C}^{B \times 1}$ is expressed as

$$\mathbf{h}_n^{P'}[i] = \begin{cases} \mathbf{h}_n^P[i] & , \mathbf{h}_n^P[i] \geq \delta \\ 0 & , otherwise \end{cases} \quad (2)$$

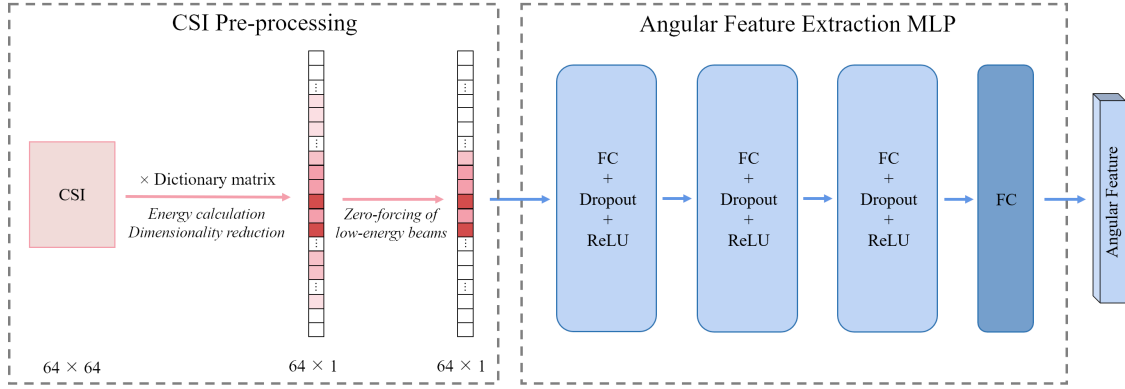


Fig. 2. Processing flow for the AFE module.

Table II gives an example of the ultimate pre-processed CSI matrix based on (1) and (2).

TABLE II
THE ULTIMATE PRE-PROCESSED CSI MATRIX.

Beam index	1	2	...	16	17	18	19	20	21	22	23	24	...	64
Ultimate values	0	0	...	0.79	0.78	0	1.69	2.42	3.27	5.26	1.69	0.81	...	0

2) *Angular Feature Extraction*: Following *dimensionality reduction* and *zero-forcing of low-energy beams*, $\mathbf{h}_n^{\text{P}'}$ is regarded as the wireless part of the multi-modal input data. To extract the angular feature from $\mathbf{h}_n^{\text{P}'}$, the AFE module adopts the multilayer perceptron (MLP) architecture which contains L_A layers. Let $\boldsymbol{\nu}_n$ be the angular feature. $\boldsymbol{\nu}_n$ is obtained by

$$\boldsymbol{\nu}_n = \text{MLP}_A(\mathbf{h}_n^{\text{P}'}, \Theta_A) = \varphi_A^{L_A}(\varphi_A^{L_A-1}(\dots\varphi_A^1(\mathbf{h}_n^{\text{P}'})\dots)) \quad (3)$$

where MLP_A represents the MLP network, $\Theta_A = \{\mathbf{W}_A, \mathbf{b}_A\}$ represents the weights and bias of the MLP network and $\varphi_A^l(\cdot)$ represents the non-linear function of the l -th layer. φ_A^l can be expressed as

$$\varphi_A^l(\mathbf{h}_n^{\text{P}'}) = f_{\text{ReLU}}(\mathbf{W}_A^l * \mathbf{h}_n^{\text{P}'} + \mathbf{b}_A^l) \quad (4)$$

where \mathbf{W}_A^l and \mathbf{b}_A^l represent the weight and bias of the l -th layer. $f_{\text{ReLU}}(\cdot)$ represents the ReLU function and can be expressed as $f_{\text{ReLU}}(x) = \max(0, x)$.

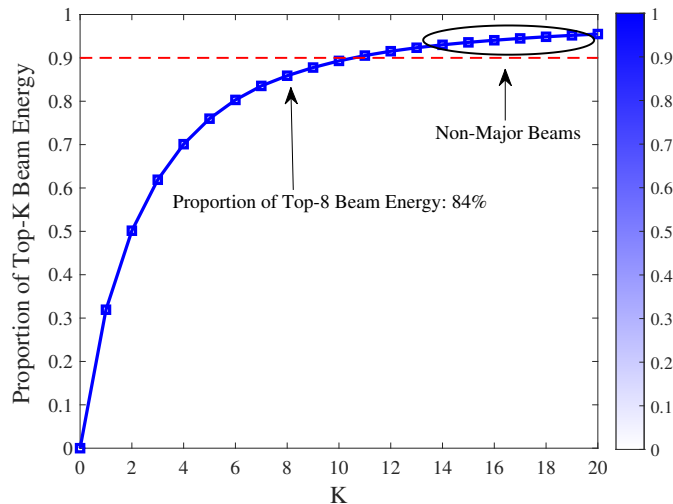


Fig. 3. Proportion of the top- k beam energy to the total energy.

For clarity, Fig. 2 shows the processing flow of the AFE module, where the CSI is first pre-processed and the angular feature is then extracted. As illustrated in Fig. 2, the proposed AFE MLP consists of three hidden layers and one output layer. Let L_A be the number of neurons in the output layer which is also the size of the angular feature and can be adaptively adjusted².

3) *Top-K Versus All*: The validity of prior CSI pre-processing is demonstrated via “*Top-K Versus All*” criterion. Specifically, the proportion of the sum of the top- k beam energy in $\mathbf{h}_n^{P'}$ to the total energy is computed. As shown in Fig. 3, the proportion dramatically increases as the number of selected beams k increases from 0 to 8. This can be attributed to the presence of a few main propagation paths between the RSU and the vehicle, with the total energy of the beams corresponding to these paths accounting for the majority of the total energy. When k is larger than 8, the proportion approaches 1 and increases slowly since the energy of the non-major beams is close to 0. As can be seen in Fig. 3, the total energy of top-8 beam energy accounts for 84% of the total energy. Consequently, only retaining the top-8 beam energy can cover the features of most propagation paths and induce a small error while significantly reducing the calculation load.

²The detailed hyper-parameters of the network architecture will be presented in Section V-C.

B. 2D-Visual Feature Extraction Module

As mentioned in Section III-A, CSI provides compressed electromagnetic environment information, and the angular feature potentially indicates the relative angle of the passing vehicle through LoS channel's azimuth. However, the location information of the vehicle provided by angular feature is relatively rough, calling for a more explicit and adequate environmental awareness as a complement. Images can visually show the location and surrounding environment of the vehicle. The global visual features of the 2D environment provided by images can benefit the localization of the vehicle and the prediction of the future position. The 2D-visual features can supplement relevant information in a non-RF format, such as the locations of scatterers. To efficiently extract the 2D-visual feature, a 2D-visual feature extraction (VFE) module is incorporated into the MMFF-Net.

1) *RGB Image Pre-processing*: Let $\mathbf{X}_n \in \mathbb{R}^{H \times W \times C}$ be the input image of the NN, where H , W and C represent the height, width and the number of color channels of the image, respectively. To adjust the values of the features in the RGB image to a similar range, the Z-score normalization is adopted to normalize the three channels of the input RGB images as

$$\hat{\mathbf{X}}_n^{(j)} = \frac{\mathbf{X}_n^{(j)} - \mu_n^{(j)}}{\sigma_n^{(j)}}, j = 1, 2, 3 \quad (5)$$

where $\hat{\mathbf{X}}_n^{(j)}$ is the j -th normalized channel, $\mu_n^{(j)}$ and $\sigma_n^{(j)}$ are the mean value and the standard deviation of the pixel value in the j -th channel, respectively. Then, the normalized RGB images are resized to 224×224 to reduce unnecessary computation for NN since there is plenty of redundant information in the original images. Let $\hat{\mathbf{X}}_n^P$ be the ultimate pre-processed RGB image.

2) *2D-Visual Feature Extraction*: After the Z-score normalization and resizing operations, $\hat{\mathbf{X}}_n^P$ is regarded as the visual part of the multi-modal input data. In the computer vision field, many powerful NNs have been designed for image feature extraction and analysis [36], serving tasks like target detection and tracking (e.g., Res-Net [37], AlexNet [38], and GoogleNet [39]). To efficiently extract the deep feature of the RGB images, the ResNet-18 [37] is adopted in VFE module for its capability of extracting more abundant features while simplifying the learning difficulty and preventing the problem of vanishing gradient. Note that the adopted ResNet-18 is customized to adaptively adjust the size of the extracted 2D-visual feature in the MMFF-Net. Specifically, the output FC layer of ResNet-18 is replaced by one with customized length L_V

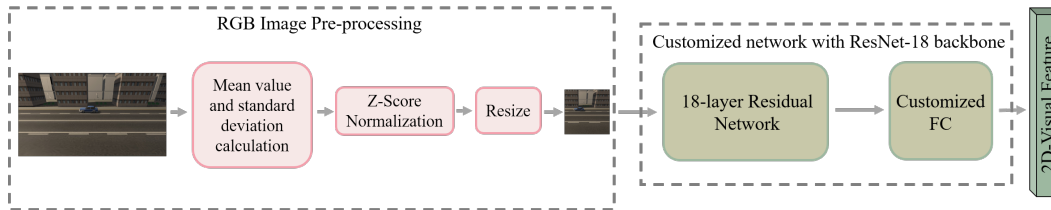


Fig. 4. Processing flow for the VFE module.

which also represents the length of the 2D-visual feature. For clarity, the processing flow for VFE module³ is shown in Fig. 4.

C. Distance Feature Extraction Module

Distance information is critical for accurate position prediction, but the AFE and VFE modules do not provide precise distance information. This lack of information limits the ability to reconstruct the 3D environment and predict the vehicle’s exact position. To address this issue, we propose incorporating radar ranging results as an essential sensing modality that naturally complements the semantic information of RGB images by providing 3D geometric shapes for 2D-visual information. To address the lack of real-world radar data in the ViWi dataset, we simulate radar sensing by adding Gaussian noise to depth maps. While the amount of distance data in simulation exceeds that of actual radar ranging, our goal is to showcase the benefits of incorporating distance information in position prediction. We will describe the pre-processing of depth maps and the extraction of distance features in the distance feature extraction (DFE) module.

1) *Depth Map Pre-processing*: At present, the processing methods of depth map is generally regarding it as an additional channel of the RGB image. This pre-processing approach is not adopted in DFE module. The reasons are as follows. First, the commonly adopted approach assumes that the distance data is accurate and ideally aligned with RGB image pixels, which is difficult to achieve by practical radar sensing. Second, distance data in depth maps are used to mimic frequent radar ranging results in this scheme. The multi-modal feature extraction and fusion method needs to be universal to radars of various operating frequencies in practical applications. To this end, the depth map is treated as an independent data source.

³The detailed hyper-parameters of the network architecture will be presented in Section V-C.

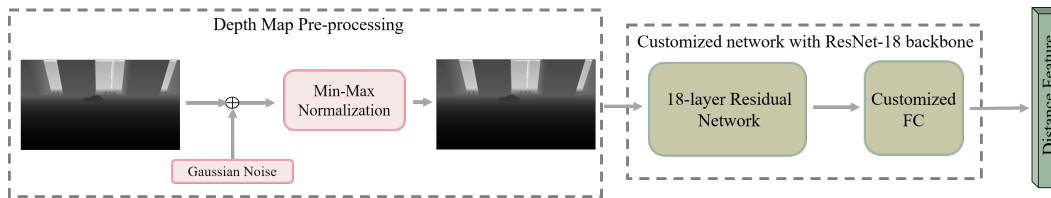


Fig. 5. Processing flow for the DFE module.

To boost the learning performance of the MMFF-Net, the order of magnitude of input multi-modal data needs to be approximately the same. Also, the values of the features in the depth map need to be adjusted to a similar range. To this end, the min-max normalization is adopted to normalize the input depth map. Let \mathbf{Y}_n , $\hat{\mathbf{Y}}_n^P$, and \mathbf{Z} be the raw, the pre-processed depth map, and Gaussian noise with zero mean and variance N_0 , respectively. N_0 is set as 0.1 in this paper. Then, the $\hat{\mathbf{Y}}_n^P$ is obtained as

$$\hat{\mathbf{Y}}_n^P = \frac{(\mathbf{Y}_n + \mathbf{Z}) - \min(\mathbf{Y}_n + \mathbf{Z})}{\max(\mathbf{Y}_n + \mathbf{Z}) - \min(\mathbf{Y}_n + \mathbf{Z})} \quad (6)$$

2) *Distance Feature Extraction*: The radar ranging results are spatially-independent discrete values. In order to make the frequent radar ranging results reflect the overall spatial structure of the environment, the radar ranging results are arranged in the form of images according to the ranging direction. In this scheme, the depth map is equivalent to the radar ranging results with spatial correlation.

Similar to the VFE module, the ResNet-18 is adopted and customized in DFE module to adaptively adjust the size of the extracted distance feature. The output FC layer of ResNet-18 is replaced by one with length L_D which also represents the length of distance feature. For clarity, the processing flow for DFE module is shown in Fig. 5.

IV. MULTI-MODAL FEATURE FUSION AND RECURRENT PREDICTION

In this section, we will introduce the fusion method for combining the angular feature, 2D-visual feature, and distance feature. After that, we will discuss the temporal feature extraction and the two regression models used in the MMFF-Net.

A. Multi-Modal Feature Fusion

The multi-modal data used in this scheme contains completely different semantic information. The 2D-visual feature, distance feature, and angular feature extracted from the VFE module,

DFE module, and AFE module, respectively, need to be preserved entirely to prevent the mixing of different features. Therefore, a tensor concatenation operation is applied to combine the three features and create an informative representation of the multi-modal feature.

Let AFE, VFE, and DFE represent the feature extraction processing of the proposed AFE module, VFE module, and DFE module, respectively. Let ν_n , χ_n , τ_n , and f_n represent the angular feature, 2D-visual feature, distance feature, and multi-modal feature, respectively. Then, the multi-modal feature fusion process can be expressed by (7a) - (7d)

$$\nu_n = \text{AFE}(\mathbf{h}_n^{P'}) \quad (7a)$$

$$\chi_n = \text{VFE}(\hat{\mathbf{X}}_n^P) \quad (7b)$$

$$\tau_n = \text{DFE}(\hat{\mathbf{Y}}_n^P) \quad (7c)$$

$$\mathbf{f}_n = \nu_n \oplus \chi_n \oplus \tau_n \quad (7d)$$

Then, the multi-modal features f_n and f_{n-1} are input into the X-axis prediction MLP and Y-axis recurrent prediction module, which will be introduced in the next subsection.

B. Temporal Feature Extraction

The motion parameters of vehicles naturally show correlation at adjacent time slots and the correlation decreases with the increase of time interval. In our scenario setting, the vehicle drifts laterally rather than moving in an ideal straight lane. Consequently, the vehicle's position tracking in this scheme is equivalent to the 2D coordinate $(\hat{x}_{n+1}, \hat{y}_{n+1})$ prediction of the vehicle. Assume that the vehicle keeps moving in a straight lane on the x -axis, and drifts laterally with a certain probability on the y -axis.

When the KF-based and the EKF-based state tracking schemes are applied to irregular motion scenarios, the tracking results when the motion state changes have large errors. To address this deficiency, we propose to extract the temporal feature of the vehicle's movement and conduct recurrent prediction of the vehicle's y -coordinates. By learning the short-term features of the vehicle's movement from the historical multi-modal data, there will be no large error in the coordinate prediction results when the vehicle drifts laterally. It is worth noting that the prediction of the vehicle's x -coordinates is not a recurrent one, since the feature of the vehicle's movement on the x -axis is easy to learn by NN. This design ensures prediction accuracy while reducing the computational load and accelerating the convergence of NN.

C. Recurrent Prediction

Long short-term memory and gated recurrent unit (GRU) networks were designed to solve the problem of vanishing gradient in recurrent neural networks for time series prediction [40]. In the MMFF-Net, GRU is adopted to extract the temporal feature of the vehicle's movement and conduct the recurrent prediction. Assume that each GRU layer contains T_u GRU units. The output of the GRU layers can be expressed as

$$F_{\text{GRU}}(\mathbf{x}^{(1)}, \mathbf{x}^{(2)}, \dots, \mathbf{x}^{(T_u)}) = (\mathbf{y}^{(1)}, \mathbf{y}^{(1)}, \dots, \mathbf{y}^{(T_u)}) \quad (8)$$

In the t -th unit of a certain layer ($1 \leq t \leq T_u$), the relationships between the input $\mathbf{x}^{(t)}$ and output $\mathbf{y}^{(t)}$ can be expressed through (9) - (12). Let $\mathbf{z}^{(t)}$ and $\mathbf{r}^{(t)}$ be the values of the t -th update gate and reset gate in GRU. f_{Sig} and f_{Tanh} represent the Sigmoid and Tanh function. Then, (9) and (10) are used to obtain $\mathbf{z}^{(t)}$ and $\mathbf{r}^{(t)}$.

$$\mathbf{z}^{(t)} = f_{\text{Sig}}(\mathbf{w}_z \mathbf{x}^{(t)} + \mathbf{u}_z \mathbf{y}^{(t-1)}) \quad (9)$$

$$\mathbf{r}^{(t)} = f_{\text{Sig}}(\mathbf{w}_r \mathbf{x}^{(t)} + \mathbf{u}_r \mathbf{y}^{(t-1)}) \quad (10)$$

where \mathbf{w}_z , \mathbf{w}_r , \mathbf{u}_z and \mathbf{u}_r are the weights and biases of the update gate and reset gate, respectively.

The information retained by the t -th unit is calculated by (11)

$$\tilde{\mathbf{o}}^{(t)} = f_{\text{Tanh}}(\mathbf{w}_o \mathbf{x}^{(t)} + \mathbf{u}_o (\mathbf{r}^{(t)} \otimes \mathbf{y}^{(t-1)})) \quad (11)$$

where \mathbf{w}_o and \mathbf{u}_o represent the linear transformations performed on $\mathbf{x}^{(t)}$ and $\mathbf{y}^{(t-1)}$, respectively.

Finally, the output of the t -th unit is calculated by (12)

$$\mathbf{o}^{(t)} = (1 - \mathbf{z}^{(t)}) \otimes \mathbf{y}^{(t-1)} + \mathbf{z}^{(t)} \otimes \tilde{\mathbf{o}}^{(t)} \quad (12)$$

In the MMFF-Net, the multi-modal data collected at the current time instance and the previous one are used to construct time series so that GRU can learn the motion feature of the vehicle. They are first input into the multi-modal feature extraction and fusion module, where the 2D-visual, distance, and angular features are extracted and fused. Then, the multi-modal feature at the current time instance is input into the X-axis prediction MLP to predict the x -coordinate. The multi-modal features from the current time instance and the previous one are stacked and input into Y-axis recurrent prediction module to predict the y -coordinate. For clarity, Fig. 6 shows the overall block diagram of the MMFF-Net.

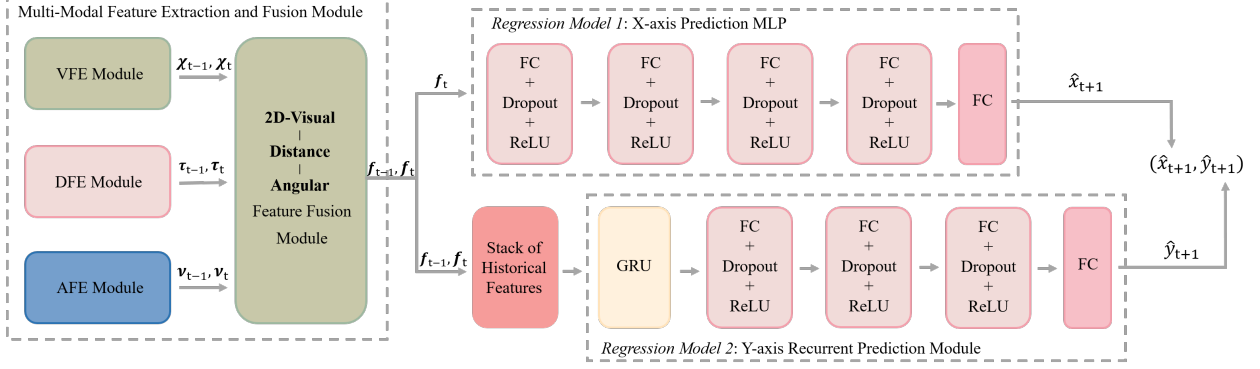


Fig. 6. The proposed MMFF-Net is composed of three main modules: (i) **multi-modal feature extraction and fusion module**, for extracting and combining the 2D-visual, distance, and angular features from the multi-modal data; (ii) **Y-axis recurrent prediction module**, for predicting the y -axis coordinate based on the stacked historical multi-modal features; and (iii) **X-axis prediction MLP**, for utilizing the multi-modal feature at the current time slot to predict the x -axis coordinate.

V. EXPERIMENTAL SETUP

This section introduces the evaluation dataset and metrics, as well as the network architecture and training methodology for MMFF-Net.

A. Dataset Overview

The dataset used for testing is based on the ViWi data-generation framework [34]. The “dist_cam” scenario acts as the basis, where a single car drives through a city street. The hyper-parameters for channel generation are presented in Table III, containing co-existing vision-wireless-distance data at each time instance. To make the dataset more realistic, the vehicle is assumed to randomly move to adjacent lanes during its movement. The complete trajectory remains continuous except for some time instances of lane changing. This randomness can also be regarded as the vehicle’s drifting. Fig. 7 displays an example of the vehicle’s trajectory where it randomly drifts.

B. Signal Model

At the n -th epoch, RSU sends a downlink directional data stream $s_n(t)$ to the vehicle using beamforming matrix $\mathbf{f}_n \in \mathbb{C}^{N_t^{\text{HF}} \times 1}$ (equivalent to the transmit beamformer for the single vehicle). The beamforming matrix \mathbf{f}_n is designed based on the intended direction. Assume that the beamforming direction $\hat{\theta}_n$ is already obtained by the proposed scheme, the beamforming matrix

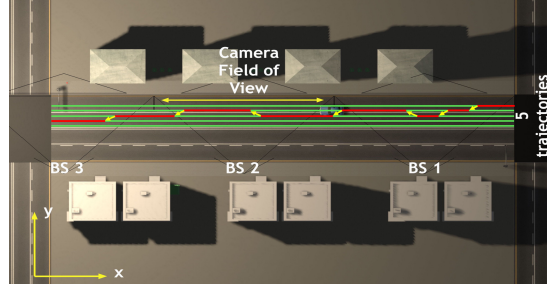


Fig. 7. An example of the vehicle's trajectory where the vehicle randomly drifts. This example is constructed based on the "dist_cam" scenario.

TABLE III
HYPER-PARAMETERS FOR CHANNEL GENERATION

Parameter	Value	
Name of scenario in ViWi [34]	dist_cam	
Active BSs	1	
Transmit antennas (x, y, z)	mmWave	(8/16/32,1,1)
	sub-6	(64,1,1)
Receive antennas (x, y, z)	mmWave	(8/16/32,1,1)
	sub-6	(1,1,1)
System bandwidth (GHz)	mmWave	2
	sub-6	0.5
Carrier frequency (GHz)	mmWave	28
	sub-6	5
Antenna spacing	0.5	
OFDM sub-carriers	mmWave	–
	sub-6	512
OFDM limit	mmWave	–
	sub-6	64
Paths	mmWave	–
	sub-6	5
Dictionary matrix size	64	

is given by $\mathbf{f}_n = \mathbf{a}(\hat{\theta}_n)$, with $\mathbf{a}(\theta) = \frac{1}{\sqrt{N_t^{\text{HF}}}} [1, e^{-j\pi \cos \theta}, \dots, e^{-j\pi(N_t^{\text{HF}}-1) \cos \theta}]^T$ representing the transmit steering vector of RSU's antenna array, which is assumed to adopt half-wavelength antenna spacing. Likewise, let $\mathbf{b}(\theta) = \frac{1}{\sqrt{M_r^{\text{HF}}}} [1, e^{-j\pi \cos \theta}, \dots, e^{-j\pi(M_r^{\text{HF}}-1) \cos \theta}]^T$ be the receive steering vector.

At the n -th epoch, the vehicle forms a receive beamformer \mathbf{w}_n according to the predicted beamforming angle to receive the signals transmitted by RSU. The receive signal is expressed

as [16]

$$c_n(t) = \tilde{\kappa} \sqrt{p_n} \alpha_n e^{j2\pi\mu_n t} \mathbf{w}_n^H \mathbf{b}(\theta_n) \mathbf{a}^H(\theta_n) \mathbf{f}_n s_n(t) + z_c(t) \quad (13)$$

where $\tilde{\kappa} = \sqrt{N_t^{\text{HF}} M_r^{\text{HF}}}$ is the antenna array gain. p_n is the transmit power, α_n is the reflection coefficient, $z_c(t)$ is the Gaussian noise term which has zero mean and variance σ_c^2 . $\mathbf{w}_n = \mathbf{b}(\hat{\theta}_n)$ is the receive beamformer that the vehicle prepares according to the predicted relative angle between the vehicle and RSU at the n -th epoch. μ_n denotes the Doppler frequency and is affected by the vehicle's velocity v_n , relative angle with RSU θ_n , and carrier frequency f_c , i.e., $\mu_n = \frac{v_n \cos \theta_n f_c}{c}$. $\alpha_n = \tilde{\alpha} d_n^{-1} e^{j\frac{2\pi f_c}{c} d_n}$ denotes the LoS channel coefficient. $\tilde{\alpha}$ representing the reference power gain factor which is assumed to be known to RSU by calculating the channel power gain at the reference distance and $\frac{2\pi f_c}{c} d_n$ represents the phase of the LoS channel.

Suppose that the transmit signal has a unit power, then the SNR of the signal received by the vehicle is given by $\text{SNR}_n = \frac{p_n |\tilde{\kappa} \alpha_n \mathbf{b}(\hat{\theta}_n)^H \mathbf{b}(\theta_n) \mathbf{a}^H(\theta_n) \mathbf{a}(\hat{\theta}_n)|^2}{\sigma_c^2}$. The achievable rate of the established link is given by $R_n = \log_2(1 + \text{SNR}_n)$. As discussed above, the achievable rate depends on the transmit and receive beamformers, which are designed based on the predicted relative angle between the vehicle and RSU. The achievable rate is maximized if the predicted beamforming angle is perfectly consistent with the actual angle, i.e., $\theta_n = \hat{\theta}_n$, yielding a SNR upper bound as $\text{SNR}_{\max} = \frac{p_n |\tilde{\kappa} \alpha_n|^2}{\sigma_c^2}$.

C. Network Configuration

Table IV shows the hyper-parameters used for designing the network, including the architecture details of the AFE MLP, the X-axis prediction MLP, and the Y-axis recurrent prediction module. On the other hand, Table V lists the hyper-parameters used for fine-tuning the model. The training of MMFF-Net is performed by PyTorch, using the adaptive moment estimation (ADAM) optimizer [41]. The network is trained for 60 epochs, with the option to use 10, 5, or 1 mini-batches in each epoch. Table IV shows the architecture of the AFE MLP, X-axis prediction MLP, and Y-axis recurrent prediction module. The AFE MLP has three hidden layers and one output layer, and the first and second dropout layers have a deactivation rate of $p = 0.2$, while the third layer has a deactivation rate of 0. The X-axis prediction MLP has four hidden layers and one output layer, with the first dropout layer having a deactivation rate of $p = 0.1$, and the other dropout layers having a deactivation rate of 0. The Y-axis recurrent prediction module has two layers of GRUs, each with r GRU units. The MLP connected to the second GRU layer has three

hidden layers and one output layer, with the first and second dropout layers having a deactivation rate of $p = 0.1$, and the third dropout layer having a deactivation rate of 0. The ReLU function serves as the activation function in the MMFF-Net. In practical applications, MMFF-Net is first trained offline and the trained model can then be deployed to RSUs with strong computing capability for online proactive beamforming. Consequently, the online proactive beamforming only requires simple calculations on low-dimensional pre-processed input data and does not bring high computation complexity.

TABLE IV
HYPER-PARAMETERS FOR NETWORK DESIGN

Parameter	Value
The size of angular feature L_A	8
The size of 2D-visual feature L_V	256
The size of distance feature L_D	256
GRU units per layer r	16
Neurons in hidden layers of AFE MLP@[layer1, layer2, layer3]	[64,32,16]
Neurons in hidden layers of X-axis Prediction MLP @[layer1, layer2, layer3, layer4]	$[L_A + L_V + L_D, 256, 128, 64]$
Neurons in hidden layers of Y-axis Recurrent Prediction module @[layer1, layer2, layer3]	[16,32,16]

TABLE V
HYPER-PARAMETERS FOR NETWORK FINE-TUNING

Parameter	Value
Batch size	[1,5,10]
Learning rate	1×10^{-3}
Learning rate scheduler	Epochs 15 and 30
Learning-rate decaying factor	0.3
Epochs	60
Data split (training-testing)	70%-30%
Optimizer	ADAM
Loss function	SmoothL1Loss

D. Benchmarks

In this paper, extensive simulation results are provided and comprehensive comparisons between the proposed scheme with several existing benchmarks are conducted. In order to highlight

the superiority and importance of multimodality fusion, three uni-modal data based schemes are designed and fine-tuned to perform the same proactive beamforming task.

- **KF-based tracking (KF-T)**: A typical KF is adopted to track the vehicle's motion parameters, where ground truth values added with noises serve as the observation values.
- **EKF-based tracking (EKF-T)** [18]: In [18], an EKF-based method is proposed where the observation values are the transmit signal echoes. The state variables are the vehicle's position and velocity, as well as the channel coefficient. Note that the commonly used state variables, angles of arrival and angles of departure, are not adopted in this scheme since they lead to high complexity in the calculation of Jacobians. The vehicle is assumed to move in an ideal straight line in the considered scenario.
- **Dual-functional radar-communication (DFRC) aided tracking (DFRC-A-T)** [19]: In [19], an EKF-based method is proposed where the DFRC signals are used for simultaneous radar sensing and communication to avoid dedicated downlink pilots. Despite the reduced signaling overhead, both the radar sensing and communication functionalities are likely to experience performance degradation when being applied to dynamic scenarios. The state variables are the vehicle's angle, distance, velocity, and reflection coefficient. The vehicle is also assumed to move in an ideal straight lane.
- **Historical trajectory points-based predictive beamforming (HTP-PB)** [24]: In [24], the vehicle's historical trajectory points and maximum likelihood estimator are used to predict the vehicle's future position. In this scheme, RSU first estimates the angle, distance of the vehicle, and the reflection coefficient, then predicts the beamforming angle based on the previous estimates. DFRC signal echoes are used as measurement values to localize and communicate with the vehicle, which introduces errors in dynamic scenarios. Without the need for a state evolution model, this scheme can be applied to more generic scenarios.
- **DL-based predictive beamforming (DL-PB)** [22]: In [22], a simple FC network is designed to estimate the current angular parameter to tackle the issue that the approximations employed in [18], [19], [24] will lead to degradation in estimation accuracy. Then, the beamforming angle at the next time slot is calculated based on the state evolution model established on the ideal straight lane. DFRC signals are also utilized and the received echoes are used as network input.

- **Vision-aided mmWave beam prediction (V-A-BP)** [25]⁴: In [25], a vision-aided mmWave beam prediction approach is proposed to predict the optimal mmWave beam directly from RGB images by degenerating the task to an image classification one. However, the pre-defined codebook is with a limited angular resolution. Therefore, the images where the vehicle is at similar positions are classified into one category. Consequently, RSU uses the same beam to communicate with the vehicle at similar positions, which inevitably leads to the deviation of beam alignment and the reduction of communication rate, especially when the antenna array is large.
- **Image-aided predictive beamforming (I-A-PB)**: A uni-modal data based scheme that utilizes images to predict the vehicle position is designed. ResNet-18 and GRU are adopted to extract the 2D-visual feature and temporal feature. These features are processed by an MLP to predict the vehicle position. The I-A-PB scheme is designed to explore the role and effect of the 2D-visual feature for vehicle position prediction.
- **Depth map-aided predictive beamforming (D-A-PB)**⁵: A uni-modal data based scheme that utilizes depth maps to predict the vehicle position is designed. The following processing methods are the same as those in the I-A-PB scheme. The D-A-PB scheme is designed to explore the role and effect of the distance feature for vehicle position prediction.
- **CSI-aided predictive beamforming (C-A-PB)**: A uni-modal data based scheme that utilizes CSI to predict the vehicle position is designed. The same data pre-processing method with the AFE module is adopted and GRU is used to extract the temporal feature. Note that the mapping between CSI and the absolute coordinates of the vehicle is difficult to fit through NN since CSI represents the compressed electromagnetic environment feature and the position of the vehicle is just one of the contributing factors. Therefore, a temporal-difference prediction scheme is designed. That is, the NN predicts the displacement of vehicles at adjacent time slots through the potential angle variation feature in CSI time series.

⁴It is worth mentioning that V-A-BP and MMFF-Net are not intended to solve the same type of problem. Therefore, adjustments are made to the reproduction of the V-A-BP under our evaluation metrics in Section VI, which may incur some fairness issues.

⁵Like the MMFF-Net, the depth map added with Gaussian noise is also used to mimic frequent radar sensing in D-A-PB scheme.

VI. PERFORMANCE EVALUATION

In this section, extensive simulation results are presented to verify the effectiveness and superiority of the proposed scheme over the benchmarks. All the simulation results presented are on the average of 500 independent realizations.

A. Angle Tracking

First, the angle tracking performance comparisons of the proposed MMFF-Net and benchmarks are given. In Fig. 8(a), the angle tracking performance of the MMFF-Net is compared with that of the KF-T, EKF-T [18], DFRC-A-T [19], and HTP-PB [24] schemes. The EKF-T, DFRC-A-T, and HTP-PB periodically utilize the received radar echoes at BS as the measurement signal vector, which causes excessive signaling overhead. The number of transmit and receive antennas affects the angle tracking accuracy. The angle prediction errors of EKF-T and HTP-PB get smaller as N_t^{HF} and M_r^{HF} increase since higher dimensional signal echoes provide more refined calibrations to the predicted values. For fair comparisons, the variances of measurement noises are set to be consistent with that given in [18], [19]. The HTP-PB performs well when the vehicle keeps moving in a straight lane but introduces large errors when the vehicle drifts laterally, as shown in Fig. 8. The performance of EKF-T is better than that of DFRC-A-T because the angle parameter used in DFRC-A-T introduces significant non-linearity and causes errors. The angle tracking error of the KF-T is also large due to its inapplicability in the non-linear motion model. The angle prediction error of EKF-T reaches the minimum of 0.0219 when $N_t^{\text{HF}} = M_r^{\text{HF}} = 32$ but it is still 8.4% higher than that of MMFF-Net. Furthermore, MMFF-Net does not consume extra signals to detect vehicle's motion status periodically and saves extensive spectrum resources. To present the angle prediction results more clearly, the relative errors are depicted in Fig. 8(b). It can be concluded that relying on the calibration of measurements can cause continuous accumulation of errors, ultimately leading to the failure of beam tracking.

Fig. 9 shows the angle tracking performances of MMFF-Net, DL-PB [22], and V-A-BP schemes [25]. The hyper-parameters for the network design and fine-tuning given in [22], [25] are adopted in our simulations. The V-A-BP predicts the optimal beam pair from a pre-defined codebook rather than tracking the angle parameter continuously. Then, the equivalent angle prediction values corresponding to the beam prediction results are obtained, which are finite discrete values due to the codebook with finite angular resolution. As can be seen in Fig. 9, the V-A-BP can only complete rough angle tracking with relatively large errors, especially when

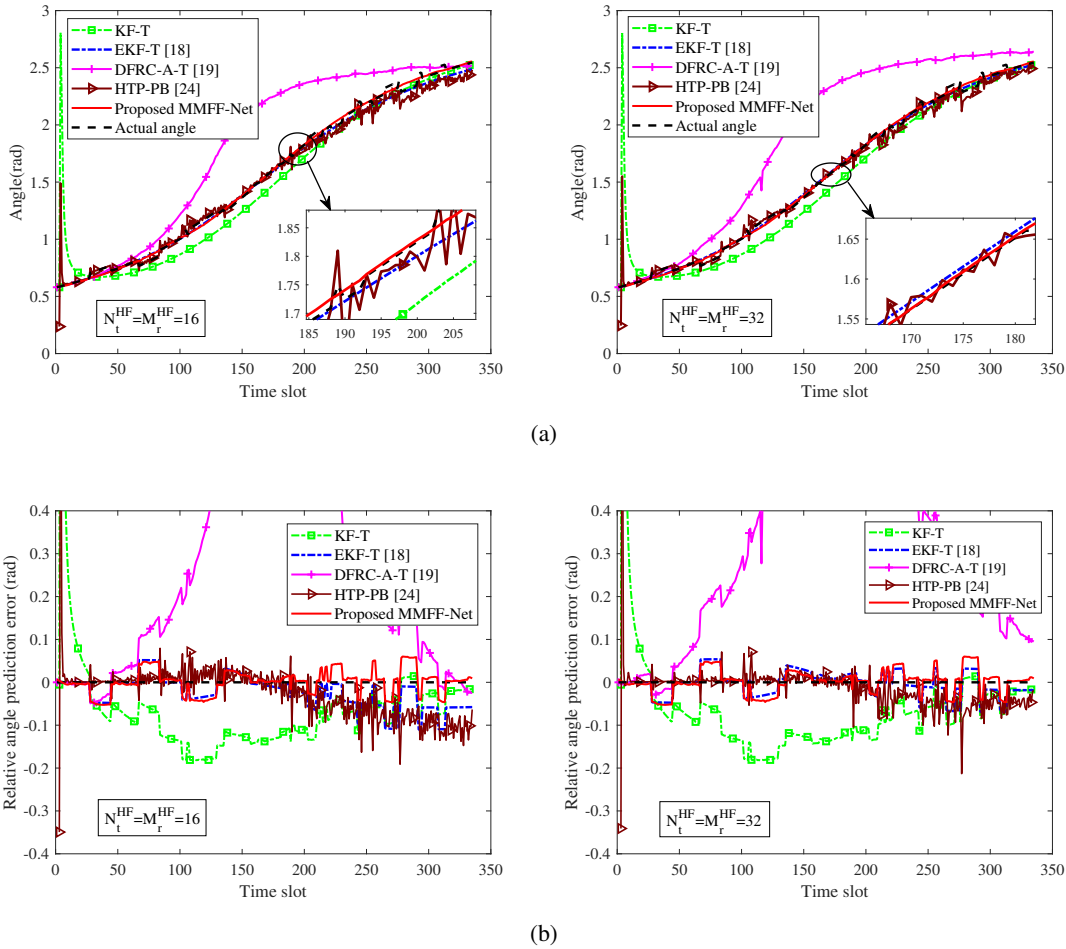


Fig. 8. Angle tracking performance comparisons among MMFF-Net, KF-T, EKF-T [18], DFRC-A-T [19], and HTP-PB [24] schemes: (a) predicted angle values achieved by these schemes; (b) relative error from actual angle.

the vehicle approaches the RSU. The DL-PB can hardly realize effective tracking of the vehicle since it merely relies on limited received signals and simple NN architecture.

To further illustrate the necessity and superiority of multimodality fusion, the performance comparison between the MMFF-Net and uni-modal schemes is presented in Fig. 10. As shown in Fig. 10(a), the C-A-PB and D-A-PB can only roughly predict the movement trend of the vehicle, which indicates that merely relying on the angular feature and distance feature is not sufficient for accurate vehicle tracking. Among the uni-modal schemes, the I-A-PB scheme performs the closest to MMFF-Net but its prediction error is still 16.8% higher. Furthermore, when the vehicle approaches RSU, the angle prediction error of I-A-PB is 42.8% higher compared with that of MMFF-Net, demonstrating its weaker tracking ability for fast-varying angles. To present the tracking results more clearly, the relative errors are depicted in Fig. 10(b). From the

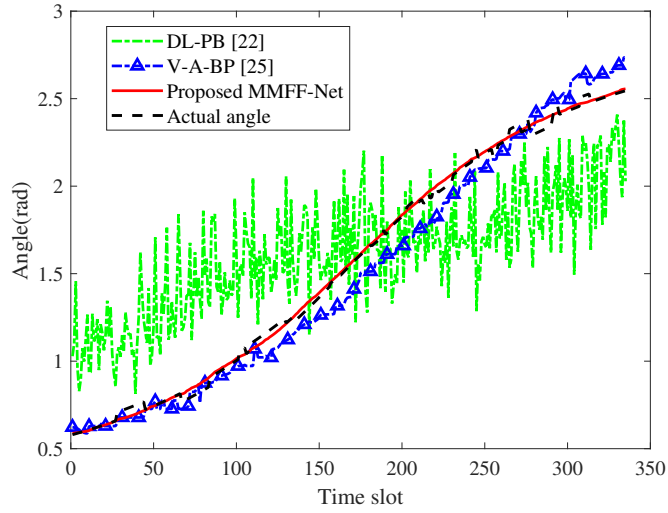


Fig. 9. Angle tracking performance comparisons among MMFF-Net, DL-PB [22], and V-A-BP [25] schemes.

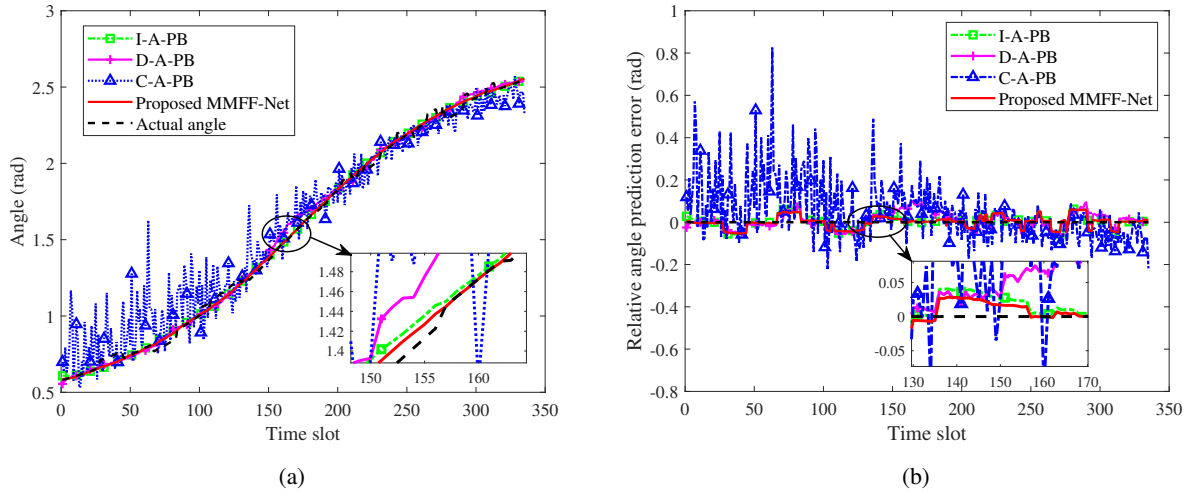


Fig. 10. Angle tracking performance comparisons between MMFF-Net and other uni-modal schemes: (a) predicted angle values achieved by these schemes; (b) relative error from actual angle.

discussion above, it can be concluded that different features can complement each other and reflect the vehicle's motion parameters more comprehensively, jointly contributing to a more accurate angle prediction result especially when the relative angle varies fast.

B. Achievable Rate

In Fig. 11, the achievable rate comparisons between MMFF-Net and several benchmark schemes are shown. The ratio of signal transmit power to noise is set to 15dB. In the simulation scenario, the vehicle travels from one side of the RSU to the other, and the distance between them decreases first and then increases. Consequently, most of the achievable rates increase first, reach the maxima when the vehicle passes RSU, and then decrease, as can be observed in Fig. 11. Furthermore, the average achievable rates increase as N_t^{HF} and M_r^{HF} increase thanks to the corresponding increased array gain. As shown in Fig. 11, the MMFF-Net and EKF-T schemes achieve similar performances in 8-antenna array case, both outperforming the three uni-modal schemes remarkably. In 16-antenna and 32-antenna array cases, the advantage of MMFF-Net over I-A-PB and EKF-T becomes notable. The average achievable rates of MMFF-Net, I-A-PB, and EKF-T are 8.21bps/Hz, 7.77bps/Hz, and 7.84bps/Hz in 16-antenna array case, and 9.20bps/Hz, 7.85bps/Hz, and 9.11bps/Hz in 32-antenna array case, respectively. Furthermore, as noted in Section VI-A, MMFF-Net possesses a stronger tracking ability for fast-varying angles, which leads to an achievable rate gain of 27.3% and 5.8% compared to I-A-PB and EKF-T when the vehicle approaches RSU in 32-antenna array case.

Fig. 11 presents the effect of vehicle drifting on achievable rate performance. The drifting behavior is realized by randomly generating a trajectory from discrete points on five parallel lanes, which is an abrupt event without any sign. Therefore, neither the uni-modal schemes nor the proposed scheme can predict such an event. The proposed scheme remains the best across the majority of the slots, despite a notable rate decrease due to misalignment in drifting, as observed in Fig. 11(b) and 11(c).

It is noteworthy that adding antennas does not necessarily ensure an increasing achievable rate. Despite the high array gain, a larger array generates a narrower beam, which is likely to miss the target vehicle and thus leads to a larger beam misalignment probability. As shown in Fig. 11, the achievable rates of the EKF-T, D-A-PB, I-A-PB, and the proposed scheme for the 16-antenna array case are higher than those of 8-antenna array case since their angle prediction accuracy can meet the alignment accuracy demand of 16-antenna array case. However, the angle prediction results of all schemes are not accurate enough to align the narrow beam generated by the 32-antenna array when the vehicle drifts, thereby causing the 32-antenna array case to perform worse than the 16-antenna array case in terms of achievable rates when the vehicle

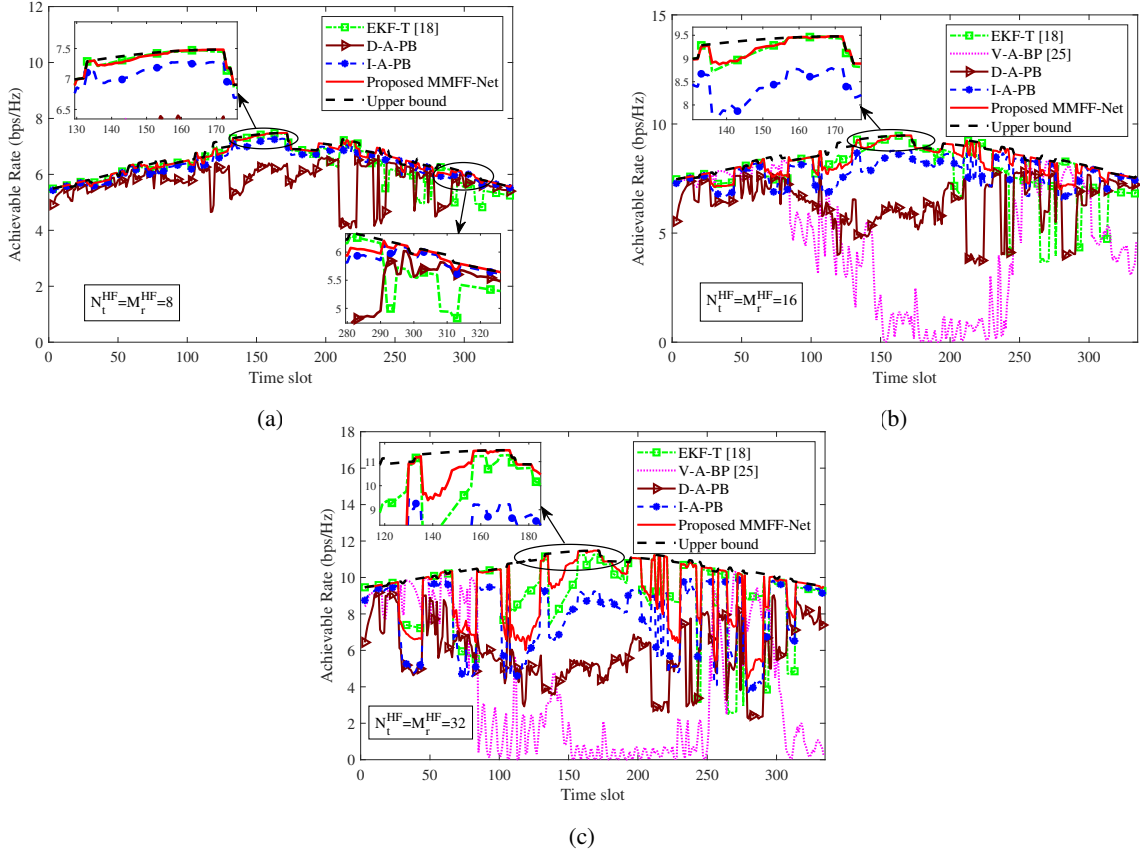


Fig. 11. Achievable rate performance comparisons among MMFF-Net, EKF-T [18], V-A-BP [25], D-A-PB, and I-A-PB schemes.

drifts.

C. Outage Probability

To evaluate the improvement of the proposed proactive beamforming scheme on the system's outage capacity, we analyze the outage probability for different beamforming approaches. Let $P(R_T)$ be the outage probability when R_T is the minimum required achievable rate, R_n be the achievable rate at the n -th time slot, $N(R_T)$ be the total number of time slots that meet the

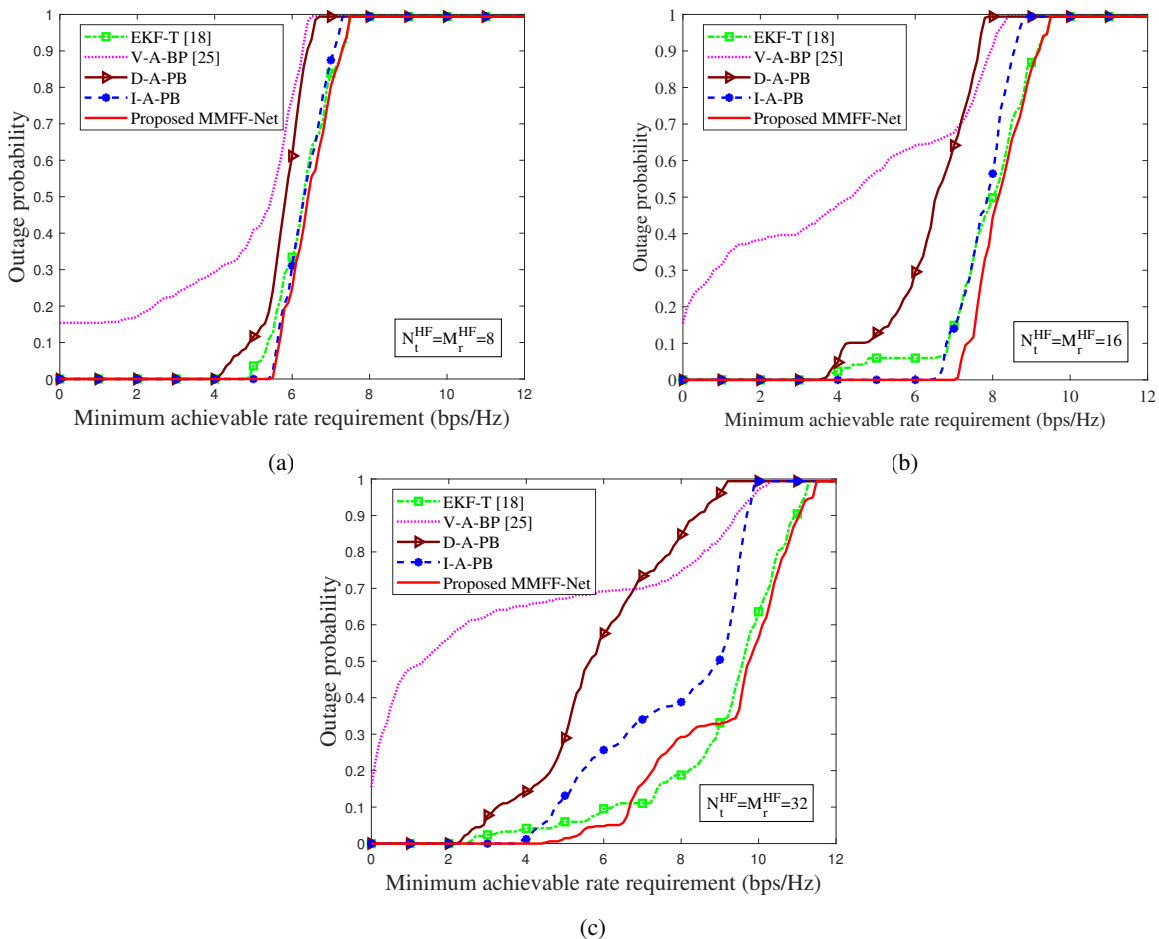


Fig. 12. Outage probability performance comparisons among MMFF-Net, EKF-T [18], V-A-BP [25], D-A-PB, and I-A-PB schemes.

minimum achievable rate demand, and N be the total number of time slots, then

$$P(R_T) = 1 - \frac{N(R_T)}{N} \quad (14a)$$

$$N(R_T) = \sum_{n=0}^N \chi(R_n, R_T) \quad (14b)$$

$$\chi(R_n, R_T) = \begin{cases} 1 & , R_n \geq R_T \\ 0 & , \text{otherwise} \end{cases} \quad (14c)$$

Fig. 12 demonstrates the proposed scheme has a lower outage probability than other schemes, with the superiority becoming evident as N_t^{HF} and M_r^{HF} increase. As discussed in Section VI-B, a larger antenna array does not necessarily lead to an increasing achievable rate since the narrower beam is more likely to miss the target vehicle. This conclusion can also be confirmed by the

outage probability of the communication system. As shown in Fig. 12(b) and 12(c), the outage probability of the 32-antenna array case is larger than that of 16-antenna array case when using the MMFF-Net, under a minimum achievable rate requirement of 4.6-7.6bps/Hz. In summary, the MMFF-Net can achieve the highest achievable rates at most conditions and keep the V2I link as stable as possible when the vehicle drifts.

VII. CONCLUSIONS

In this paper, we presented a novel proactive beamforming scheme for V2I links that leverages multi-modal sensing and communication integration. Our proposed scheme takes advantage of the complementary nature of multi-modal environment information and captures distinct features of the surrounding environment. To effectively extract and fuse the multi-modal features implied by the multi-modal data, we designed a novel MMFF-Net capable of pre-processing the multi-modal data with distinct data structures in the form of time series. To demonstrate the applicability of the proposed scheme to complex and dynamic scenarios, we constructed a dataset using the ViWi data-generation framework and enriched it by considering the vehicle's drifting behavior. We compared our proposed scheme with nine representative methods and found that it outperformed them in terms of angle prediction accuracy, achievable rate, and outage performance, especially when the relative angle varies rapidly. Moreover, our proposed scheme exhibited the strongest robustness against vehicle drifting, demonstrating its practicality and effectiveness in complex dynamic scenarios.

REFERENCES

- [1] W. Xu *et al.*, "Internet of Vehicles in big data era," *IEEE/CAA J. Automat. Sinica*, vol. 5, no. 1, pp. 19–35, Jan. 2018.
- [2] N. Lu, N. Cheng, N. Zhang, X. Shen, and J. W. Mark, "Connected Vehicles: Solutions and Challenges," *IEEE Internet Things J.*, vol. 1, no. 4, pp. 289–299, Aug. 2014.
- [3] X. Cheng, D. Duan, S. Gao, and L. Yang, "Integrated Sensing and Communications (ISAC) for Vehicular Communication Networks (VCN)," *IEEE Internet Things J.*, vol. 9, no. 23, pp. 23441–23451, Dec. 2022.
- [4] S. Chen *et al.*, "Vehicle-to-Everything (v2x) Services Supported by LTE-Based Systems and 5G," *IEEE Commun. Stand. Mag.*, vol. 1, no. 2, pp. 70–76, 2017.
- [5] X. Cheng, S. Gao, and L. Yang, *mmWave Massive MIMO Vehicular Communications*. Springer, Nature, Switzerland, 2022.
- [6] F. Boccardi, R. W. Heath, A. Lozano, T. L. Marzetta, and P. Popovski, "Five disruptive technology directions for 5G," *IEEE Commun. Mag.*, vol. 52, no. 2, pp. 74–80, Feb. 2014.
- [7] F. Rusek, D. Persson, B. K. Lau, E. G. Larsson, T. L. Marzetta, O. Edfors, and F. Tufvesson, "Scaling Up MIMO: Opportunities and Challenges with Very Large Arrays," *IEEE Signal Process. Mag.*, vol. 30, no. 1, pp. 40–60, Jan. 2013.

- [8] K. V. Mishra, M. R. B. Shankar, V. Koivunen, B. Ottersten, and S. A. Vorobyov, "Toward millimeter wave joint radar-communications: A signal processing perspective," *IEEE Signal Process. Mag.*, vol. 36, no. 5, pp. 100–114, Sep. 2019.
- [9] O. El Ayach, S. Rajagopal, S. Abu-Surra, Z. Pi, and R. W. Heath, "Spatially Sparse Precoding in Millimeter Wave MIMO Systems," *IEEE Trans. Wireless Commun.*, vol. 13, no. 3, pp. 1499–1513, Mar. 2014.
- [10] S. Gao, X. Cheng, and L. Yang, "Mutual Information Maximizing Wideband Multi-User (wMU) mmWave Massive MIMO," *IEEE Trans. Commun.*, vol. 69, no. 5, pp. 3067–3078, May. 2021.
- [11] T. Van Luong, N. Shlezinger, C. Xu, T. M. Hoang, Y. C. Eldar, and L. Hanzo, "Deep Learning Based Successive Interference Cancellation for the Non-Orthogonal Downlink," *IEEE Trans. Veh. Technol.*, vol. 71, no. 11, pp. 11876–11888, Nov. 2022.
- [12] J. Wang *et al.*, "Beam codebook based beamforming protocol for multi-Gbps millimeter-wave WPAN systems," *IEEE J. Select. Areas Commun.*, vol. 27, no. 8, pp. 1390–1399, Oct. 2009.
- [13] Z. Xiao, T. He, P. Xia, and X.-G. Xia, "Hierarchical Codebook Design for Beamforming Training in Millimeter-Wave Communication," *IEEE Trans. Wireless Commun.*, vol. 15, no. 5, pp. 3380–3392, May. 2016.
- [14] V. Va, H. Vikalo, and R. W. Heath, "Beam tracking for mobile millimeter wave communication systems," in *2016 IEEE Global Conference on Signal and Information Processing (GlobalSIP)*, Washington, DC, USA, Dec. 2016, pp. 743–747.
- [15] A. Alkhateeb, O. El Ayach, G. Leus, and R. W. Heath, "Channel Estimation and Hybrid Precoding for Millimeter Wave Cellular Systems," *IEEE J. Sel. Top. Sign. Proces.*, vol. 8, no. 5, pp. 831–846, Oct. 2014.
- [16] S. Gao, X. Cheng, and L. Yang, "Estimating Doubly-Selective Channels for Hybrid mmWave Massive MIMO Systems: A Doubly-Sparse Approach," *IEEE Trans. Wireless Commun.*, vol. 19, no. 9, pp. 5703–5715, Sep. 2020.
- [17] X. Cheng, Z. Huang, and L. Bai, "Channel Nonstationarity and Consistency for Beyond 5G and 6G: A Survey," *IEEE Commun. Surveys Tutor.*, vol. 24, no. 3, pp. 1634–1669, 3rd Quart., 2022.
- [18] S. Shaham, M. Ding, M. Kokshoorn, Z. Lin, S. Dang, and R. Abbas, "Fast Channel Estimation and Beam Tracking for Millimeter Wave Vehicular Communications," *IEEE Access*, vol. 7, pp. 141104–141118, 2019.
- [19] F. Liu, W. Yuan, C. Masouros, and J. Yuan, "Radar-Assisted Predictive Beamforming for Vehicular Links: Communication Served by Sensing," *IEEE Trans. Wireless Commun.*, vol. 19, no. 11, pp. 7704–7719, Nov. 2020.
- [20] W. Yuan, F. Liu, C. Masouros, J. Yuan, D. W. K. Ng, and N. González-Prelcic, "Bayesian Predictive Beamforming for Vehicular Networks: A Low-Overhead Joint Radar-Communication Approach," *IEEE Trans. Wireless Commun.*, vol. 20, no. 3, pp. 1442–1456, Mar. 2021.
- [21] W. Yuan, Z. Wei, S. Li, J. Yuan, and D. W. K. Ng, "Integrated Sensing and Communication-Assisted Orthogonal Time Frequency Space Transmission for Vehicular Networks," *IEEE J. Sel. Top. Sign. Proces.*, vol. 15, no. 6, pp. 1515–1528, Nov. 2021.
- [22] J. Mu, Y. Gong, F. Zhang, Y. Cui, F. Zheng, and X. Jing, "Integrated Sensing and Communication-Enabled Predictive Beamforming With Deep Learning in Vehicular Networks," *IEEE Commun. Lett.*, vol. 25, no. 10, pp. 3301–3304, Oct. 2021.
- [23] C. Liu, W. Yuan, S. Li, X. Liu, H. Li, D. K. Ng, and Y. Li, "Learning-Based Predictive Beamforming for Integrated Sensing and Communication in Vehicular Networks," *IEEE J. Select. Areas Commun.*, vol. 40, no. 80, pp. 2317–2334, Aug. 2022.
- [24] F. Liu and C. Masouros, "A Tutorial on Joint Radar and Communication Transmission for Vehicular Networks—Part III: Predictive Beamforming Without State Models," *IEEE Commun. Lett.*, vol. 25, no. 2, pp. 332–336, Feb. 2021.
- [25] M. Alrabeiah, A. Hredzak, and A. Alkhateeb, "Millimeter Wave Base Stations with Cameras: Vision-Aided Beam and Blockage Prediction," in *Proc. VTC-Spring*, Antwerp, Belgium, May. 2020, pp. 1–5.
- [26] U. Demirhan and A. Alkhateeb, "Radar Aided 6G Beam Prediction: Deep Learning Algorithms and Real-World Demonstration," in *Proc. WCNC*, Austin, TX, USA, Apr. 2022, pp. 2655–2660.

- [27] A. Klautau, N. González-Prelcic, and R. W. Heath, "LIDAR Data for Deep Learning-Based mmWave Beam-Selection," *IEEE Wireless Commun. Lett.*, vol. 8, no. 3, pp. 909–912, Jun. 2019.
- [28] S. Wu, C. Chakrabarti, and A. Alkhateeb, "LiDAR-Aided Mobile Blockage Prediction in Real-World Millimeter Wave Systems," in *Proc. WCNC*, Austin, TX, USA, Apr. 2022, pp. 2631–2636.
- [29] W. Xu, F. Gao, J. Zhang, X. Tao, and A. Alkhateeb, "Deep Learning Based Channel Covariance Matrix Estimation With User Location and Scene Images," *IEEE Trans. Commun.*, vol. 69, no. 12, pp. 8145–8158, Dec. 2021.
- [30] G. Charan, M. Alrabeiah, and A. Alkhateeb, "Vision-Aided 6G Wireless Communications: Blockage Prediction and Proactive Handoff," *IEEE Trans. Veh. Technol.*, vol. 70, no. 10, pp. 10193–10208, Oct. 2021.
- [31] S. Huang, M. Zhang, Y. Gao, and Z. Feng, "MIMO Radar Aided mmWave Time-Varying Channel Estimation in MU-MIMO V2X Communications," *IEEE Trans. Wireless Commun.*, vol. 20, no. 11, pp. 7581–7594, Nov. 2021.
- [32] Y. Fan, S. Gao, D. Duan, X. Cheng, and L. Yang, "Radar Integrated MIMO Communications for Multi-Hop V2V Networking," *IEEE Wireless Commun. Lett.*, vol. 12, no. 2, pp. 307–311, Feb. 2023.
- [33] W. Xu, F. Gao, X. Tao, J. Zhang, and A. Alkhateeb, "Computer Vision Aided mmWave Beam Alignment in V2X Communications," *IEEE Trans. Wireless Commun.*, vol. 22, no. 4, pp. 2699–2714, Apr. 2023.
- [34] M. Alrabeiah, A. Hredzak, Z. Liu, and A. Alkhateeb, "ViWi: A Deep Learning Dataset Framework for Vision-Aided Wireless Communications," in *Proc. IEEE 91st Vehicular Technol. Conf. (VTC2020-Spring)*, Antwerp, Belgium, May. 2020, pp. 1–5.
- [35] F. Gao, B. Lin, C. Bian, T. Zhou, J. Qian, and H. Wang, "FusionNet: Enhanced Beam Prediction for mmWave Communications Using Sub-6 GHz Channel and a Few Pilots," *IEEE Trans. Commun.*, vol. 69, no. 12, pp. 8488–8500, Dec. 2021.
- [36] J. Ngiam, A. Khosla, M. Kim, J. Nam, H. Lee, and A. Ng, "Multimodal deep learning," *Proc. ICML*, Jan. 2011, pp. 689–696.
- [37] K. He, X. Zhang, S. Ren, and J. Sun, "Deep Residual Learning for Image Recognition," in *Proc. IEEE Conf. Comput. Vis. Pattern Recognit. (CVPR)*, Las Vegas, NV, USA, Jun. 2016, pp. 770–778.
- [38] A. Krizhevsky, I. Sutskever, and G. E. Hinton, "Imagenet classification with deep convolutional neural networks," in *Proc. Int. Conf. Neural Inf. Process. Syst. (NIPS)*, Lake Tahoe, NV, USA, Dec. 2012, pp. 1097–1105.
- [39] C. Szegedy, *et al.*, "Going deeper with convolutions," in *Proc. IEEE Conf. Comput. Vis. Pattern Recognit. (CVPR)*, Boston, MA, USA, Jun. 2015, pp. 1–9.
- [40] I. Goodfellow, Y. Bengio, and A. Courville, *Deep Learning*. Cambridge, MA, USA: MIT Press, 2016.
- [41] D. P. Kingma and J. Ba, "Adam: A method for stochastic optimization," in *Proc. Int. Conf. Learn. Representations*, 2015.